

# Gradient Modulus Strategy for Alleviating Stretchable Electronic Strain Concentration

Boning Sun, Zemin Li, Zhuoyu Song, Yang Yu, Zhonglong Zhang, Runhui Zhou, Boru Jin, Ziyu Chen, Yushu Wang, Jiang He, Rongrong Bao,\* Wenchao Gao,\* and Caofeng Pan\*

The island-bridge structural design is a common strategy for imparting stretchability to flexible electronic devices. In this structure, the low modulus regions bear most of the deformation, while the rigid islands, which house the electronic components, undergo minimal deformation. However, due to the modulus differences that can be several times or even several orders of magnitude larger, severe strain concentration occur at the edges of the rigid islands in high modulus regions. This strain concentration caused by rigid constraints not only reduces the stretchability of the soft substrate but also degrades the mechanical performance of the interconnected structures, thereby significantly affecting the overall stability of the device. Starting from finite element simulations, this paper introduces modulus gradient regions and optimizes geometric parameters, significantly alleviating the strain concentration at the edges of the rigid islands. Serpentine-shaped circuits are then transferred to a substrate with strain isolation, which demonstrates better stretchability stability under 20% elongation compared to traditional strain isolation strategies. In addition, the stretchable light emitting diode (LED) system with gradient modulus has better stretchability compared to the system with conventional strategy. This suggests that this strategy has great potential in maintaining the stability of stretchable systems.

broad application potential in fields such as tactile sensing,<sup>[1]</sup> health monitoring,<sup>[2]</sup> and artificial bionic devices.<sup>[3]</sup> Achieving stretchability in electronic devices typically involves advancements in both material and structural aspects. Structural stretchability is applicable to various existing material systems, offering broad versatility and convenience. This approach includes intricate geometric engineering (such as zigzag, serpentine, and helical shapes) and structural design strategies (such as kirigami structures, buckling structures, and island-bridge structures). These methods allow traditional rigid electronic components to resist mechanical deformation, bypassing the need for the development of high-performance materials that are intrinsically stretchable. Among these strategies, the island-bridge structure is a widely applied method that combines elastic substrates with non-stretchable rigid electronic components, achieving direct integration of traditional electronic devices into stretchable electronics.<sup>[4]</sup> In this design, rigid

## 1. Introduction

Stretchable electronics technology overcomes the inherent brittleness of traditional electronic devices, thereby demonstrating

electronic components are placed in high-modulus areas (the “islands”). When the whole system is subjected to stretching, most of the strain is borne by the low-modulus substrate region, thereby protecting the rigid electronic components from high

B. Sun, Y. Yu, Z. Zhang, B. Jin, Z. Chen, Y. Wang, C. Pan  
Center on Nanoenergy Research  
Institute of Science and Technology for Carbon Peak & Neutrality  
Key Laboratory of Blue Energy and Systems Integration (Guangxi University)  
Education Department of Guangxi Zhuang Autonomous Region  
School of Physical Science & Technology  
Guangxi University  
Nanning 530004, P. R. China  
E-mail: [pancaofeng@buaa.edu.cn](mailto:pancaofeng@buaa.edu.cn)

B. Sun, Z. Li, Y. Yu, Z. Zhang, R. Zhou, B. Jin, Z. Chen, Y. Wang, J. He, R. Bao, W. Gao, C. Pan  
Beijing Institute of Nanoenergy and Nanosystems  
Chinese Academy of Sciences  
Beijing 101400, P. R. China  
E-mail: [baorongrong@binn.cas.cn](mailto:baorongrong@binn.cas.cn); [gaowenchao@binn.cas.cn](mailto:gaowenchao@binn.cas.cn)

Z. Li, R. Zhou  
School of Nanoscience and Engineering  
University of Chinese Academy of Sciences  
Beijing 100049, P. R. China

Z. Song  
Department of Engineering Mechanics  
Dalian University of Technology  
Dalian 116024, P. R. China

R. Bao, C. Pan  
Institute of Atomic Manufacturing  
Beihang University  
Beijing 100191, P. R. China

 The ORCID identification number(s) for the author(s) of this article can be found under <https://doi.org/10.1002/adfm.202410676>

DOI: 10.1002/adfm.202410676

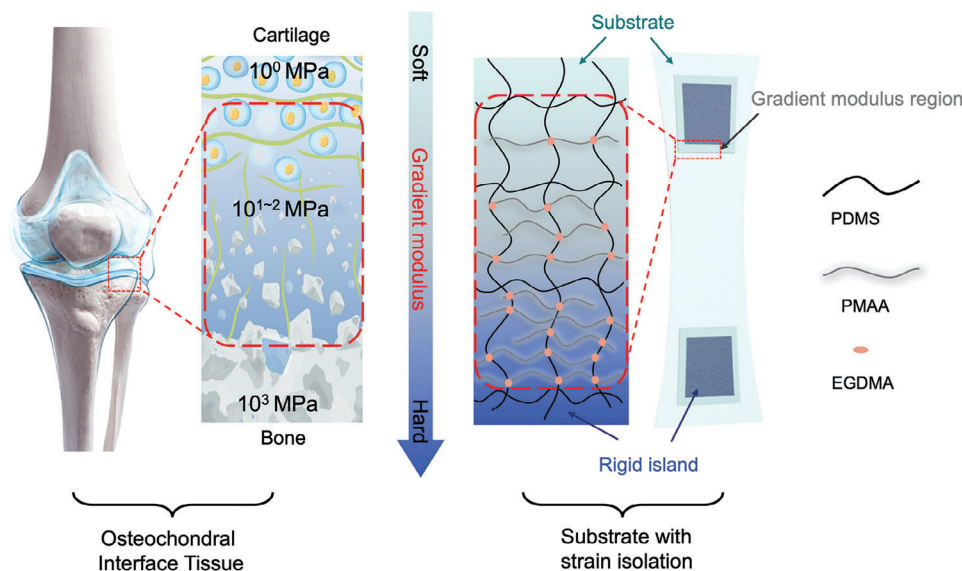


**Figure 1.** Gradient Modulus Strategy Design: Biomimetic Gradient Modulus Transition Zone Inspired by Bone-Cartilage Interface.

strain, achieving strain isolation. This method significantly enhances the tensile performance of the devices, providing crucial technical support for the development of stretchable electronics technology.

However, the modulus mismatch between the rigid islands and the elastomeric substrate in island-bridge structures often leads to strain concentration at the interface, a phenomenon that has been reported in many studies.<sup>[4e,5]</sup> Strain concentration causes uneven stress distribution in the substrate during stretching, leading to localized regions reaching the elastic strain limit under relatively small macroscopic strain, thus reducing the stretchability of the device.<sup>[6]</sup> Similar issues are known as stress concentration of inclusions in fields such as composite materials, and have been extensively studied.<sup>[7]</sup>

To alleviate strain concentration issues, several studies have explored the deposition of rigid layers with varying moduli in a layer-by-layer manner on a stretchable electronic substrate. This approach forms rigid islands with vertically oriented gradient moduli, a strategy that has been shown to significantly mitigate strain concentration on the substrate.<sup>[4b,8]</sup> In recent years, methods such as oxidation and secondary curing have been extensively studied for their ability to in situ form programmable rigid islands on the substrate.<sup>[4c,9]</sup> Unlike the direct deposition of rigid islands on the substrate, these methods offer advantages such as ease of operation and high pattern accuracy. However, despite the increasing application of these in situ formed rigid islands in stretchable electronics, theoretical analysis of their strain concentration issues and solutions remains limited.

This study is inspired by the bone-cartilage interface in the human body, as shown in **Figure 1**. The bone-cartilage interface features a fine organic-inorganic compositional gradient, forming a modulus transition zone ( $10^0$ – $10^3$  MPa), ensuring effective mechanical conduction despite enduring millions of mechanical load cycles.<sup>[10]</sup> Similarly, to mitigate strain concentration in island-bridge structures, this study introduces a gradient modulus structure as a transition between the rigid island and the

soft substrate, creating a continuous buffer zone between the two moduli. The modulus near the rigid island is similar to it, while the modulus near the soft substrate is lower but slightly higher than that of the soft substrate. In our research, we optimized the parameters of this structure through finite element simulation and obtained substrates with gradient modulus structures via gradient photopolymerization. Additionally, we tested substrates with serpentine-shaped interconnected structures and stretchable LED devices, verifying the effectiveness of this gradient modulus strategy.

## 2. Results and Discussion

### 2.1. Finite Element Simulation and Parameter Optimization of Gradient Modulus Structure

In island-bridge structures, the elastic modulus of the rigid island is typically an order of magnitude higher than that of the soft substrate to achieve strain isolation. This level of modulus difference can be approximated as strain concentration caused by rigid constraints. To explore the capability of this structure in mitigating strain concentration, it is essential to systematically investigate the impact of size parameters on strain concentration in soft substrates with rigid islands. Using the widely applied square rigid island as an example (as shown in **Figure 2A**), a  $2 \times 2$  array of square rigid islands was designed, each with an annular modulus transition zone at the junction with the soft substrate. Finite element simulations (**Figure 2B**) show that the soft substrate with a modulus transition zone exhibits a maximum stress of 92.3% under 50% uniaxial stretching, where the traditional rigid island soft substrate (without a modulus transition zone) exhibits a maximum strain of 122.2%, which is 30% higher. By normalizing the finite element simulation results at the edge of the rigid island, a distance-strain curve was obtained, as shown in **Figure 2C**. It was found that the maximum strain in the strain concentration zone of the substrate with a gradient modulus was reduced, further

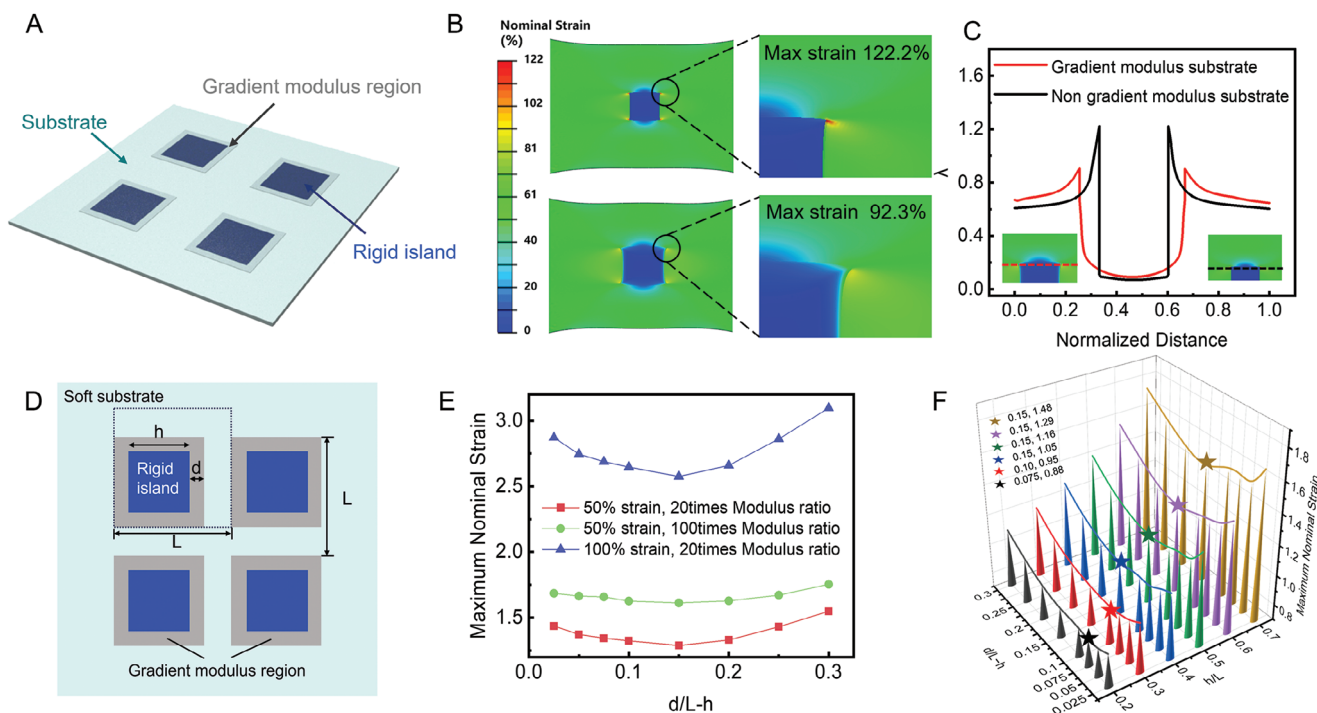


**Figure 2.** Finite Element Analysis (FEA) of Gradient Modulus Structures and Parameter Optimization. A) Structural Model Used for FEA Optimization. B) Strain Distribution Simulation of Substrates with and without Gradient Modulus Structures. C) Surface Strain Comparison of Substrates with and without Gradient Modulus. D) Geometric Parameters of Gradient Modulus Substrates. E) Relationship Between Different Dimensional Parameters and Maximum Strain under 50% Stretching and modulus ratio of 20:1. F) Relationship Between Dimensional Parameters and Relative Width of Gradient Modulus under 50% Stretching with modulus ratio of 20:1, 50% Stretching with a modulus ratio of 100:1, and 100% Stretching with 20 times Modulus Ratio.

confirming that substrates with a modulus gradient can significantly alleviate strain concentration at the edges of rigid islands.

To optimize the parameters of the gradient modulus region and identify suitable gradient modulus dimensions for stretchable electronics, it is first necessary to parametrize the geometric features of a typical rigid island array. As shown in Figure 2D, the rigid islands periodically arranged on the substrate have distinct characteristics: period  $L$ , width of the rigid island  $h$ , and width of the gradient modulus region  $d$ . When considering the rigid islands as a form of rigid constraint, the maximum strain of the substrate to be studied is determined by the average strain of the soft substrate and the strain concentration caused by the rigid constraint on the substrate. The average strain can be estimated using an empirical formula:

$$\bar{\epsilon} = \epsilon_{app} \frac{L}{L-h} \quad (1)$$

In this formula,  $\epsilon_{app}$  is the applied strain on the substrate. Thus, the expression for the maximum strain  $\epsilon_{max}$  can be derived:

$$\epsilon_{max} = K \bar{\epsilon} = K \epsilon_{app} \frac{1}{1 - \frac{h}{L}} \quad (2)$$

where  $K$  is the stress concentration factor, which is a dimensionless constant that, under constant applied strain and rigid

island modulus, depends only on the shape of the rigid island. For square rigid islands with a gradient modulus, the magnitude of the stress concentration factor  $K$  is only related to the relative width of the gradient modulus region  $d/(L-h)$ . Hence,  $\epsilon_{max}$  is determined by the relative width of the rigid island's period  $h/L$  and  $d/(L-h)$ . It is noteworthy that the parameter  $h/L$  is often determined by practical application requirements. Therefore, in this work, we investigate the effect of the relative width of the gradient modulus region  $d/(L-h)$  on the maximum strain of the substrate under different  $h/L$  values to explore the impact of gradient modulus structures on strain concentration.

Based on finite element simulations, we first studied the relationship between the maximum strain on the substrate surface and the width of the gradient modulus region when the width of the rigid island relative to the period length ( $h/L$ ) is 0.6. As shown in Figure 2E, the entire substrate with a modulus ratio of 20:1 (the ratio of rigid islands to substrates) was subjected to 50% and 100% stretching, whereas the substrate with a modulus ratio of 100:1 underwent 50% stretching. Under these three conditions, the maximum strain exhibited a consistent pattern, with the lowest maximum strain on the substrate surface occurring when the relative width of the gradient modulus region was 0.15. Figure S1 (Supporting Information) shows the finite element simulation for a modulus ratio of 20:1 and 50% substrate stretching, where the relative width of the gradient modulus region is 0.15.

In order to further explore the rule of change between the parameters when the relative width of the rigid island changes, 48 models were built for each of these three cases respectively, as shown in Figure 2F and Figure S1, and S2 (Supporting Information). When  $h/L$  is 0.4, 0.5, 0.6, and 0.7, all three scenarios show the lowest maximum strain on the substrate surface occurring at a gradient modulus region width of 0.15. However, when  $h/L$  is 0.2 and 0.3, the lowest maximum strain occurs at gradient modulus region widths of 0.1 and 0.075, respectively. This indicates that when the relative width of the rigid island to the period is moderate or large, the optimal relative width of the gradient modulus structure is 0.15; when the relative width of the rigid island to the period is small, the optimal relative width of the gradient modulus structure also decreases accordingly. Additionally, Figure S2C (Supporting Information) shows the surface strain curves of gradient modulus structures with different relative widths along the dashed line shown in Figure S2D (Supporting Information) when  $h/L = 0.5$ , the modulus ratio is 20:1, and substrate stretching is 50%. From this, it can be inferred that a wider gradient modulus region leads to smaller local strains, thereby gradually mitigating strain concentration issues. There exists an optimal relative width parameter that allows the gradient modulus structure to minimize the maximum strain on the substrate surface to the greatest extent.

## 2.2. Preparation and Characterization of Gradient Modulus Substrates

Polydimethylsiloxane (PDMS) is widely used in the field of stretchable electronics due to its dielectric properties, transparency, and biocompatibility.<sup>[11]</sup> One primary method for creating strain-isolating substrates with PDMS is to mix benzophenone into the uncured PDMS, followed by ultraviolet (UV) exposure.<sup>[9a,b,12]</sup> Another method is to add a resin monomer solution to the PDMS and then perform UV exposure.<sup>[9c]</sup> Although the latter method involves more complex steps, it achieves better soft-hard differentiation and stronger strain isolation. Therefore, this study chose to use the latter process. As shown in the process flow of Figure 3A, the uncured PDMS is first adhered to a glass substrate coated with a polyimide (Pi) layer, then soaked in a Methacrylic Acid (MAA) monomer for 30 min, followed by 2 min of UV exposure under a mask, and finally, the PDMS film is peeled off from the substrate.

To achieve varying degrees of curing in the modulus transition zone of PDMS and obtain a strain-isolating substrate with a modulus gradient, we used inkjet printing technology to create a gradient transparency mask, as shown in Figure S3A,B (Supporting Information). The transparency gradually decreases from the center of the rigid island (fully transparent) outward, resulting in decreasing curing levels upon UV exposure, thus forming a gradient modulus zone that ultimately connects to the soft substrate. The obtained substrate is shown in Figure 3B.

Raman characterization of the rigid island and soft substrate areas revealed the presence of characteristic carboxyl peaks ( $966$  and  $1451\text{ cm}^{-1}$ ) in the rigid island region crosslinked and cured with Polymethyl Methacrylate (Figure 3C). Subsequent Raman scans from the rigid island area toward the soft substrate area,

it was observed that the substrate with the gradient modulus zone showed a gradual decrease in the intensity of the carboxyl peak at  $966\text{ cm}^{-1}$  with distance (Figure 3D, Where  $x$  is the coordinate of the displacement table in the test). In contrast, the substrate without the gradient modulus zone only showed the carboxyl peak in the rigid island area (Figure S4, Supporting Information), indicating that the substrate with a compositional gradient was successfully prepared using the gradient transparency mask. Subsequently, we prepared substrates with different gradient moduli using templates with varying numbers of transparent layers to investigate the effect of gradient variation rate on the overall mechanical performance of the substrate. As shown in Figure 3E, with an increase in the number of printing layers, the gradient variation rate decreased, resulting in a smoother modulus transition between the soft and hard areas, and the overall modulus of the substrate gradually decreased, exhibiting more flexible mechanical properties. The stress-strain curves of substrates with different printing layers shown in Figure S5 (Supporting Information) also corroborate this point.

To further verify, a gold film was uniformly magnetron-sputtered on both substrates, followed by 20% uniaxial stretching. As seen in Figure 3E, the substrate with the gradient modulus transition zone exhibited fewer and smaller cracks compared to the substrate without this transition zone. For a more detailed analysis, the areas of cracks in different regions of the two substrates were statistically analyzed (Figure 3F). The crack areas in the rigid island region of both substrates were almost the same, but in the middle region of the substrate, the substrate with the gradient modulus transition zone had 19% more higher cracks compared to the substrate without the transition zone (Figure 3G). However, at the annular edge region of the rigid island, the substrate with the gradient modulus transition zone had 29% smaller crack areas than the substrate without the transition zone. The crack area represents the strain level on the substrate surface. The results show that the maximum strain on the substrate surface with the gradient modulus transition zone was significantly reduced compared to the substrate without the transition zone, further indicating that this strategy significantly alleviates strain concentration.

## 2.3. The Influence of Modulus Gradient Substrate on Interconnect Structure

From the above investigation, it is evident that substrates incorporating gradient modulus transition zones can significantly reduce local strain and enhance the overall tensile properties of the substrate. To study the effect of the gradient modulus strategy on interconnected structures, as shown in Figure 4A, serpentine-shaped circuits were fabricated on two types of substrates (with and without gradient modulus zones) to connect two rigid islands. Figure S7 (Supporting Information) shows the physical image of the obtained device. In addition, environmental exposure tests were conducted on the device (Figure S8, Supporting Information). Under 10% strain, as the metal fatigue of the electrodes is not significant under such low strain, the electrodes on both substrates exhibited similar stability during cyclic testing (Figure S9A,B, Supporting

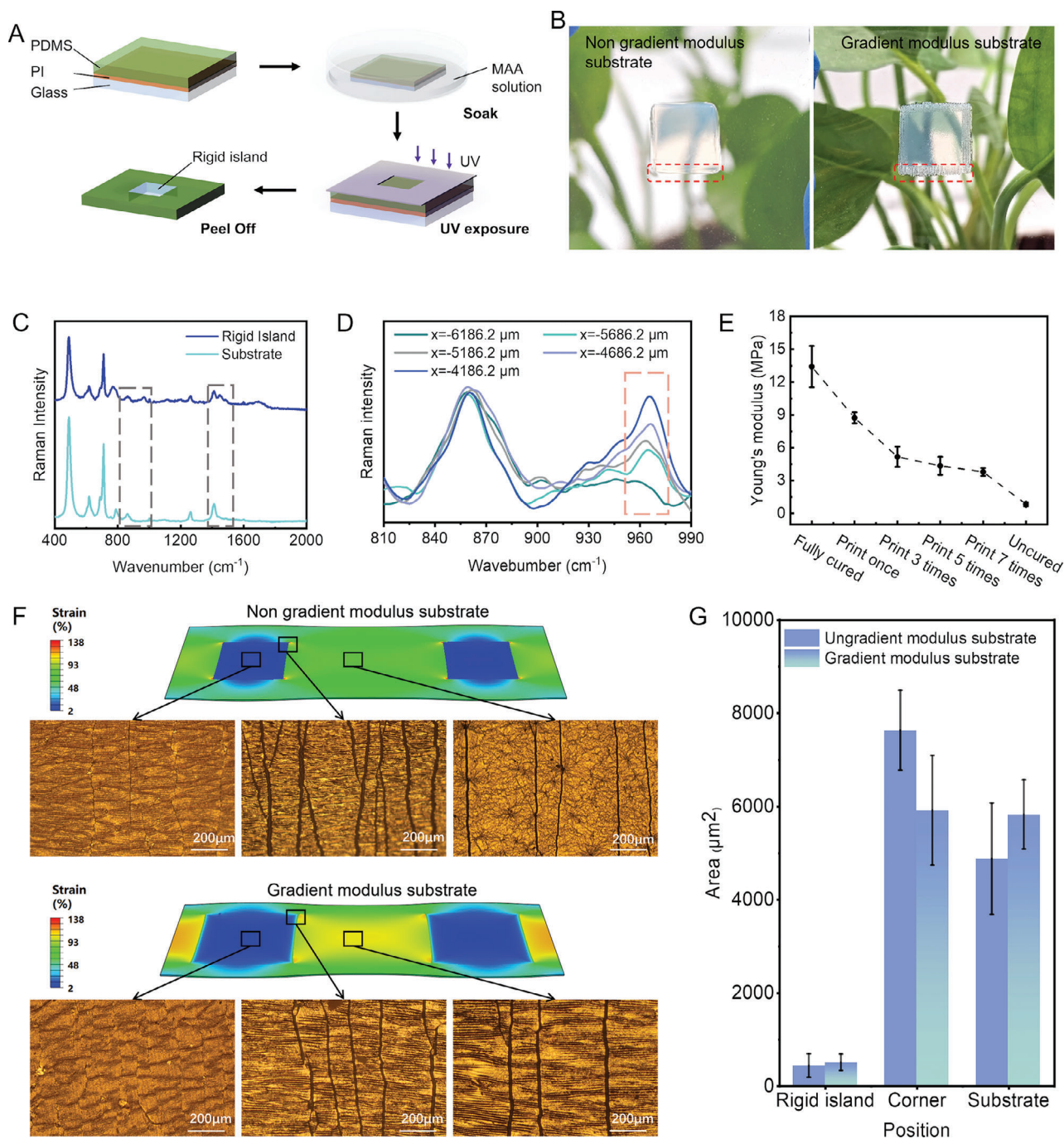


**Figure 3.** Preparation and Characterization of Gradient Modulus Substrates. A) Preparation Process of Gradient Modulus Substrates. B) Photographs of Substrates with and without Gradient Modulus. C) Raman Characterization of Soft Substrate and Rigid Island. D) Raman Spectra of Gradient Modulus Zone from Rigid Island to Soft Substrate. E) Young's Modulus of Different Curing Conditions in Gradient Modulus Zone. F) Strain Distribution and Optical Micrographs of Cracks in Gold Film of Various Regions after 20% Stretching of Substrates with and without Gradient Modulus. G) Crack Area Statistics of Two Types of Substrates.

Information). Upon applying 20% strain, it was observed that the substrate with the gradient modulus zone maintained a stable relative resistance change value after 1 000 cycles, whereas the substrate without the transition zone exhibited irregular fluctuations, with the maximum value exceeding the normal value ( $\Delta R/R_0 = 0.3$ ) by nearly four times (Figure 4B). This indicates

that the soft substrate with the gradient modulus transition zone can maintain the mechanical stability of the interconnected structure. The impact of the two types of substrates on the interconnected structure was studied using finite element simulations. As shown in Figure 4C, after 50% stretching, the maximum stress of the interconnected structure combined with the

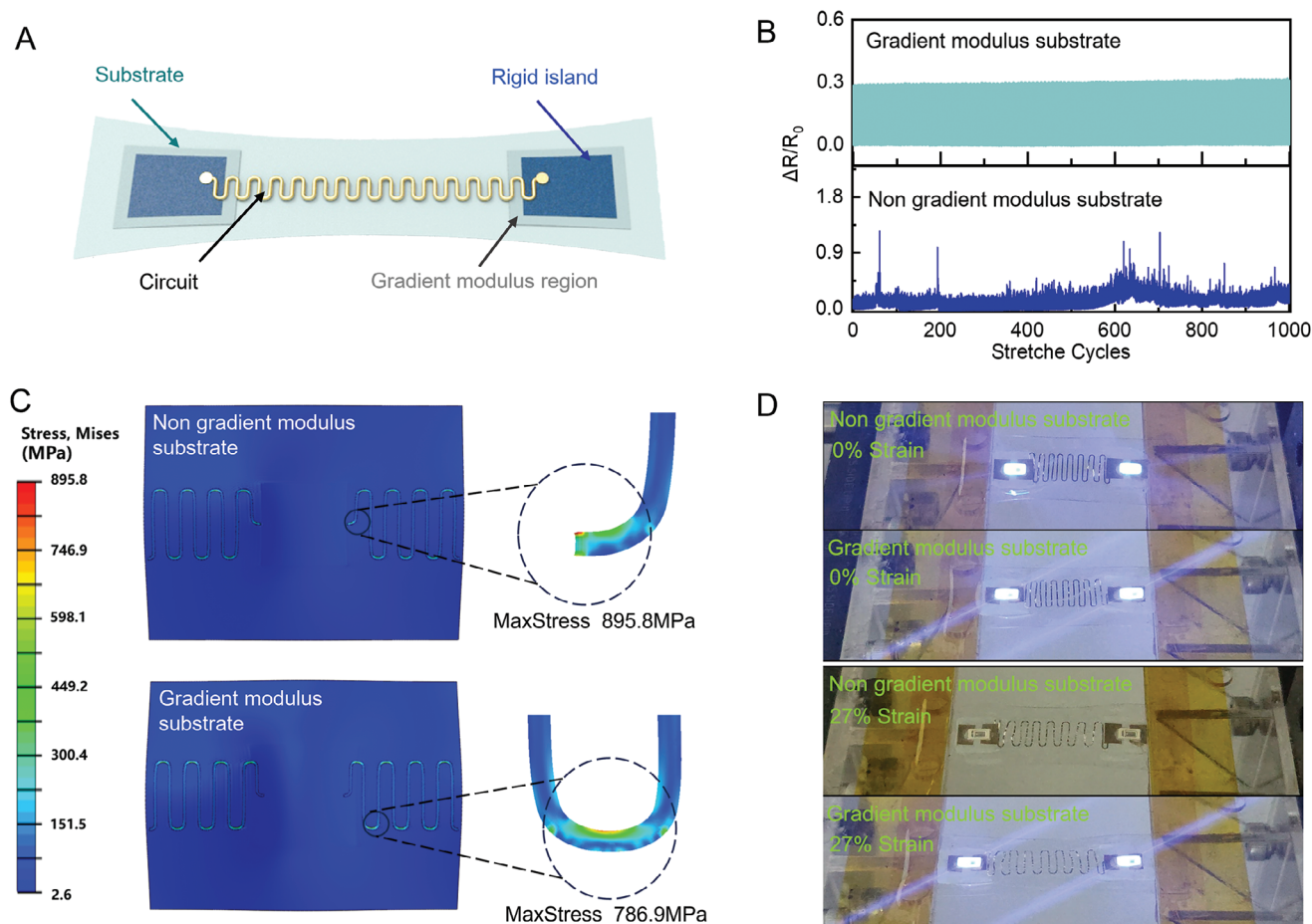


**Figure 4.** Effect of Gradient Modulus Substrates on Interconnect Structures. A) Gradient Modulus Substrates with Serpentine Circuits. B) Stretching Cycle Stability of Serpentine Electrodes on Substrates with and without Gradient Modulus (20% stretch). C) Stress Distribution Simulation of Serpentine Circuits on Substrates with and without Gradient Modulus (50% stretch). D) Conductive State of Circuits under Stretching on Substrates with and without Gradient Modulus after Connecting LEDs.

substrate without the gradient modulus was 895.8 MPa, occurring at the junction with the rigid island, consistent with previously reported cases.<sup>[5b,7]</sup> In contrast, the maximum stress point of the interconnected structure combined with the gradient modulus substrate shifted to a bend away from the rigid island, with the maximum stress being 786.9 MPa, a 12% reduction compared to the structure without the gradient modulus. The lower stress under the same stretching conditions alleviated the fatigue failure of the serpentine line, providing the device with better mechanical stability.

Subsequently, LEDs were placed on the rigid islands on both sides, and constant-speed strain was applied to both types of devices. The substrate without the gradient modulus transition zone experienced local instability at 27% strain, causing the LED to extinguish, whereas the substrate with the transition zone could continue to stretch up to 32% strain, an 18% increase (Figure 4D; Video S1, Supporting Information). This demonstrates that the strategy can mitigate strain concentration and shows significant potential for maintaining the stability of stretchable sensor systems.

### 3. Conclusion

This paper utilizes finite element simulation as a theoretical guide, combined with structural design and experimental verification, to propose a strategy for mitigating strain concentration caused by rigid islands in stretchable electronics. By using a gradient transparency mask, a gradient modulus region is formed between the photopolymerized rigid island and the soft substrate. This method alleviates strain concentration caused by modulus discontinuities at the interface by expanding the spatial scale of modulus variation, thereby preventing premature substrate failure due to local strain limits during stretching. Additionally, this paper employs finite element calculation to study the impact of gradient modulus regions on strain concentration, explores the optimal geometric dimensions for mitigating strain concentration, and provides general design principles for gradient modulus region dimensions. Specifically, when the rigid island distribution density is normal or high, the width of the gradient modulus region should be 15% of the spacing between rigid islands; when the density is low, the optimal width should decrease accordingly. Finally, by combining serpentine electrodes and

simple LED devices, the ability of gradient modulus design to mitigate fatigue failure in interconnected structures were studied, demonstrating the application potential of gradient modulus design in stretchable electronics.

## 4. Experimental Section

**Finite Element Analysis:** Finite Element Analysis (FEA) was conducted using the commercial software ABAQUS2020. The elastic substrate and its rigid islands were modeled using 8-node linear bricks with reduced integration and hourglass control, while the serpentine electrodes were modeled using 4-node doubly curved thin or thick shells with reduced integration, hourglass control, and finite membrane strains. The elastic substrate and rigid islands both used a linear elastic model, with  $E_{\text{soft}} = 0.625$  MPa,  $\nu_{\text{soft}} = 0.29$ ,  $E_{\text{hard}} = 12.5$  MPa,  $\nu_{\text{hard}} = 0.29$ , and  $E_{\text{pi}} = 3$  GPa,  $\nu_{\text{pi}} = 0.30$ . The modulus gradient in the transition region between the elastic substrate and the rigid islands was set using a keyword-associated script file, with the script data calculated based on the spatial relationships of the mesh. All model meshes were sufficiently refined. The serpentine electrodes were predefined to be constrained on the upper surface of the elastic substrate and subjected to uniaxial stretching along with the elastic substrate.

**Preparation of Gradient Light-Transmitting Mask:** Apply a commercial circuit printing coating solution (BroadTeko CT-PT) onto a glass substrate using a spin coating (600 rpm for 30 s), then place it on a hotplate and bake at 80 °C for 10 min. Use AutoCAD2022 to draw five concentric hollow square patterns with side lengths of 1, 1.05, 1.1, 1.15, and 1.2 cm, respectively, and convert them into TIFF format. Align the prepared glass substrate with the coating solution in the circuit printer (BroadTeko DP800) and print the pre-drawn patterns from the previous step layer by layer on the substrate with silver ink (BroadCON-INK550). After each layer was printed, use a handheld heat gun to bake it at 150 °C for 30 s. After all layers are printed, place the mask on a hotplate and bake it at 120 °C for 1 h. The final gradient light-transmitting mask is shown in the figure.

**Preparation of Elastic Substrate:** Spin-coat PDMS, mixed in a 15:1 ratio of base agent to curing agent, onto an appropriate glass substrate (1 000 rpm for 30 s), and cured it at 60 °C for 6 h. Peel the PDMS elastic substrate from the glass, soak the elastic substrate in an MAA monomer mixed with 3% w/w ethylene glycol dimethacrylate and 1% w/w Irgacure 651 for 20 min, then remove it. Next, place the gradient light-transmitting mask on the upper surface of the PDMS and use PI-coated glass as the substrate on the lower surface of the PDMS. Expose it to UV light (15 mW cm<sup>-2</sup>) for 2 min in a glove box to obtain rigid islands with a modulus gradient. Substrates without a gradient modulus were prepared using a standard mask.

**Serpentine Electrode Fabrication Process:** Spin-coat a 10% w/w dextran solution onto a glass substrate (600 rpm for 30 s), bake at 80 °C for 1 h, and then attach a 6 μm PI tape as the substrate on the dextran layer. Perform photolithography and magnetron sputtering to deposit a gold layer (thickness ≈ 100 μm) on the glass-PI substrate, and then perform lift-off to obtain the serpentine-patterned gold film. Then, remove the unprotected PI layer by dry etching to obtain serpentine-patterned gold-PI electrodes. Release the electrodes in water and transfer them onto the elastic substrate.

**Stretchable LED System Fabrication:** The fabrication of the stretchable LED system begins with the preparation of elastic substrates with and without gradient modulus (thickness ≈ 1 mm). After transferring the serpentine electrodes onto the elastic substrate, LEDs (models: 0402, 0603, 0805, 1206, and 3528) were bonded to the serpentine interconnect electrodes using conductive silver paste and nickel cloth (FS05001). The assembly was then encapsulated with PDMS mixed in a 15:1 ratio of base agent to curing agent (1 000 rpm for 30 s) and cured at 60 °C for 6 h.

**Experimental characterization:** Uniaxial tensile tests on the substrate were conducted using a tensile machine (YL-S71, Yuelian). The crack area of the substrate was characterized using an optical microscope (Zeiss Observer Z1) and Image-Pro Plus 6.0. The Raman spectrum of the substrate was characterized and tested using a confocal Raman spectrometer

(LabRAM HR Evolution, HORIBA) equipped with a 50× lens and a 532 nm laser. The stability and uniaxial tensile tests of the serpentine electrode and LED system were conducted using a linear motor (Linmot E1100/LinMot) and an LCR meter (E4980A, Agilent). The stretching speed was 10 mm s<sup>-1</sup>. During the resistance test, the positive and negative copper wires at the ends of the electrodes are connected to the two furniture of the LCR meter, and the test channel was Rx. The positive and negative copper wires were connected to the two ends of the serpentine electrode via silver paste.

## Supporting Information

Supporting Information is available from the Wiley Online Library or from the author.

## Acknowledgements

B.N.S., Z.M.L., and Z.Y.S. contributed equally to this work. The authors thank the support of National Natural Science Foundation of China (No. 52203307), National Science Foundation of Beijing (L223006 and 2222088), National Natural Science Foundation of China (No. 52125205, U20A20166, 61805015, 61804011, 52202181 and 52102184), the National Key R&D Program of China (2021YFB3200302 and 2021YFB3200304), the Shenzhen Science and Technology Program (KQTD20170810105439418) and the Fundamental Research Funds for the Central Universities for their support.

## Conflict of Interest

The authors declare no conflict of interest.

## Data Availability Statement

The data that support the findings of this study are available from the corresponding author upon reasonable request.

## Keywords

island-bridge structural, polydimethylsiloxane, strain concentration, stretchable electronics

Received: June 18, 2024  
Revised: September 24, 2024  
Published online: October 8, 2024

- [1] a) K. Zhou, Y. Zhao, X. Sun, Z. Yuan, G. Zheng, K. Dai, L. Mi, C. Pan, C. Liu, C. Shen, *Nano Energy* **2020**, *70*, 104546; b) J. He, R. Wei, S. Ge, W. Wu, J. Guo, J. Tao, R. Wang, C. Wang, C. Pan, *InfoMat* **2024**, *6*, 12493; c) R. Bao, J. Tao, J. Zhao, M. Dong, J. Li, C. Pan, *Sci. Bull.* **2023**, *68*, 1027; d) Y. Lu, X. Qu, W. Zhao, Y. Ren, W. Si, W. Wang, Q. Wang, W. Huang, X. Dong, *Research* **2020**, *2020*, 2038560; e) C. Wang, L. Dong, D. Peng, C. Pan, *Adv. Intell. Syst.* **2019**, *1*, 1900090.
- [2] a) K. Zhou, W. Xu, Y. Yu, W. Zhai, Z. Yuan, K. Dai, G. Zheng, L. Mi, C. Pan, C. Liu, *Small* **2021**, *17*, 2100542; b) R. Zhu, Z. Li, G. Deng, Y. Yu, J. Shui, R. Yu, C. Pan, X. Liu, *Nano Energy* **2022**, *92*, 106700; c) J. He, R. Zhou, Y. Zhang, W. Gao, T. Chen, W. Mai, C. Pan, *Adv. Funct. Mater.* **2022**, *32*, 2107281; d) Q. Zhou, S. Deng, A. Gao, B. Wang, J. Lai, J. Pan, L. Huang, C. Pan, G. Meng, F. Xia, *Adv. Funct. Mater.* **2023**, *33*, 2306619; e) W. Gao, J. Huang, J. He, R. Zhou, Z. Li, Z. Chen, Y. Zhang, C. Pan, *InfoMat* **2023**, *5*, 12426; f) G. Ge, Y. Lu, X. Qu, W. Zhao, Y. Ren, W. Wang, Q. Wang, W. Huang, X. Dong, *ACS Nano* **2019**, *14*, 218; g) G. Ge, W. Yuan, W. Zhao, Y. Lu, Y. Zhang, W. Wang, P. Chen, W. Huang, W. Si, X. Dong, *J. Mater. Chem. A* **2019**, *7*, 5949.

- [3] a) C. Ma, M. Wang, K. Wang, P. C. Uzabakiriho, X. Chen, G. Zhao, *Adv. Fiber. Mater.* **2023**, *5*, 1392; b) S. Chun, D. W. Kim, S. Baik, H. J. Lee, J. H. Lee, S. H. Bhang, C. Pang, *Adv. Funct. Mater.* **2018**, *28*, 1805224; c) C. Wang, H. Hu, D. Zhu, C. Pan, *Sci. Bull.* **2023**, *68*, 559; d) W. Wu, X. Han, J. Li, X. Wang, Y. Zhang, Z. Huo, Q. Chen, X. Sun, Z. Xu, Y. Tan, *Adv. Mater.* **2021**, *33*, 2006006.
- [4] a) J. C. Yang, S. Lee, B. S. Ma, J. Kim, M. Song, S. Y. Kim, D. W. Kim, T.-S. Kim, S. Park, *Sci. Adv.* **2022**, *8*, eabn3863; b) Y. Kim, J. Kim, C. Y. Kim, T. Kim, C. Lee, K. Jeong, W. Jo, S. Yoo, T.-S. Kim, K. C. Choi, *Chem. Eng. J.* **2022**, *431*, 134074; c) Y. Cao, G. Zhang, Y. Zhang, M. Yue, Y. Chen, S. Cai, T. Xie, X. Feng, *Adv. Funct. Mater.* **2018**, *28*, 1804604; d) Y. Li, N. Li, W. Liu, A. Prominski, S. Kang, Y. Dai, Y. Liu, H. Hu, S. Wai, S. Dai, *Nat. Commun.* **2023**, *14*, 4488; e) M. Wang, K. Wang, C. Ma, P. C. Uzabakiriho, X. Chen, G. Zhao, *ACS Appl. Mater. Interfaces.* **2022**, *14*, 35997.
- [5] a) H. Li, Z. Wang, S. Lu, Y. Ma, X. Feng, *Adv. Mater. Technol.* **2019**, *4*, 1800365; b) K. Li, X. Cheng, F. Zhu, L. Li, Z. Xie, H. Luan, Z. Wang, Z. Ji, H. Wang, F. Liu, *Adv. Funct. Mater.* **2019**, *29*, 1806630. c) Y. Liu, Z. Liu, B. Zhu, J. Yu, K. He, W. R. Leow, M. Wang, B. K. Chandran, D. Qi, H. Wang, *Adv. Mater.* **2017**, *29*, 1701780; d) Y. Nishio, J. Hirotsu, S. Kishimoto, H. Kataura, Y. Ohno, *Adv. Electron. Mater.* **2021**, *7*, 2000674.
- [6] a) K. Li, Y. Shuai, X. Cheng, H. Luan, S. Liu, C. Yang, Z. Xue, Y. Huang, Y. Zhang, *Small.* **2022**, *18*, 2107879. b) N. Matsuhisa, M. Kaltenbrunner, T. Yokota, H. Jinno, K. Kuribara, T. Sekitani, T. Someya, *Nat. Commun.* **2015**, *6*, 7461.
- [7] a) X. Frank, K. Lampoh, J.-Y. Delenne, *Phys. Rev. E.* **2023**, *108*, 034903; b) D. Y. Yevgeny, G. V. e. Lasko, *Engineering.* **2012**, *4*, 583; c) Y. Chen, *Theor. Appl. Fract. Mech.* **2016**, *84*, 177; d) M. Myneni, K. R. Rajagopal, *Math. Mech. Solids.* **2023**, *28*, 394.
- [8] R. Libanori, R. M. Erb, A. Reiser, H. L.e Ferrand, M. J. Süess, R. Spolenak, A. R. Studart, *Nat. Commun.* **2012**, *3*, 1265.
- [9] a) M. Cai, S. Nie, Y. Du, C. Wang, J. Song, *ACS Appl. Mater. Interfaces.* **2019**, *11*, 14340; b) S. Pan, Z. Liu, M. Wang, Y. Jiang, Y. Luo, C. Wan, D. Qi, C. Wang, X. Ge, X. Chen, *Adv. Mater.* **2019**, *31*, 1903130; c) H. G. Park, M. Kim, H. Park, J. H. Oh, *Adv. Funct. Mater.* **2024**, *34*, 2312034; d) J. Cui, R. Xu, W. Dong, T. Kaneko, M. Chen, D. Shi, *ACS Appl. Mater. Interfaces.* **2023**, *15*, 48736; e) E. Li, Z. Rao, X. Wang, Y. Liu, R. Yu, G. Chen, H. Chen, T. Guo, *IEEE Electron. Dev. Lett.* **2021**, *42*, 1484; f) L. Miao, H. Guo, J. Wan, H. Wang, Y. Song, H. Chen, X. Chen, H. Zhang, *J. Micromech. Microeng.* **2020**, *30*, 045001.
- [10] X. Wang, J. Lin, Z. Li, Y. Ma, X. Zhang, Q. He, Q. Wu, Y. Yan, W. Wei, X. Yao, *Nano Lett.* **2022**, *22*, 2309.
- [11] a) F. Wang, Z.-Q. Gao, C.-P. Feng, D.-Y. Wang, M.-P. Jin, F. Zhang, Z.-L. Peng, G.-M. Zhang, X.-Y. Zhu, H.-B. Lan, *Addit. Manuf.* **2024**, *81*, 103985; b) D. Xu, L. Sun, Z. Zhang, Y. Wang, X. Zhang, F. Ye, Y. Zhao, J. Pan, *Appl. Mater. Today.* **2021**, *24*, 101124; c) F. Li, X. Wang, Z. Xia, C. Pan, Q. Liu, *Adv. Funct. Mater.* **2017**, *27*, 1700051; d) D. Qi, K. Zhang, G. Tian, B. Jiang, Y. Huang, *Adv. Mater.* **2021**, *33*, 2003155.
- [12] S. Gandla, H. Gupta, A. R. Pininti, A. Tewari, D. Gupta, *RSC Adv.* **2016**, *6*, 107793.